



Dynamic changes in mangroves of the largest delta in northern Beibu Gulf, China: Reasons and causes

Chuqi Long^a, Zhijun Dai^{a,b,*}, Riming Wang^c, Yaying Lou^a, Xiaoyan Zhou^a, Shushi Li^c, Yuhua Nie^d

^a State Key Laboratory of Estuarine and Coastal Research, East China Normal University, Shanghai, China

^b Southern Marine Science and Engineering Guangdong Laboratory (Zhuhai), Zhuhai 519080, Guangdong, China

^c Key Laboratory of Coastal Science and Engineering/Qinzhou Key Laboratory for Eco-Restoration of Environment, Beibu Gulf University, Guangxi 535011, China

^d South China Sea Information Center of State Oceanic Administration, China

ARTICLE INFO

Keywords:

Mangrove forests
Suspended sediment discharge
Estuarine hydrodynamics
Nanliu River Delta of Beibu Gulf
Anthropogenic activities
Sea level rise

ABSTRACT

Many mangrove forests occur along estuaries and deltas are experiencing irreparable losses throughout the world due to changes in natural factors and intensive anthropogenic interferences. However, little information is available regarding variations in mangrove forests and associated reasons and causes. Here, the long-term dynamic patterns of mangrove forests in the Nanliu River Delta (NRD), the largest delta in the Beibu Gulf, China, were detected based on a series of hydrosediment data and remote sensing images between 1986 and 2020. The results indicated that the total mangrove forest area of the NRD increased in an incremental manner, even though a rapid decline occurred in the western terrestrial margin of the delta before 1998. Additionally, mangrove forests have expanded southeastward to the sea in the eastern NRD, and they have colonized to the southwest in the western NRD. Moreover, long-lasting horizontal seaward expansion with vertical accretion in the bare tidal flat of the NRD created new sites for potential mangrove regeneration. Furthermore, an average annual sea level rise of 0.2 mm per year and an 86% decline in fluvial sediment supply could not cause expansions and local losses of mangrove forests. The combination of local tidal currents and waves transports sufficient estuarine sediment to the northeast into the delta to provide important sediment material for the deposition of mangrove tidal flats. The mangrove forest destruction induced by local residents and the ecological restoration implemented by the government are the causes of the continuous serious losses and extensive gains of mangrove forests, respectively. The results highlighted that the dynamic changes in mangrove forests in the NRD caused by driving forces from natural and human interferences can serve as significant references for mangrove forest restoration and decision-making policy management in similar deltas around the world.

1. Introduction

Mangroves are salt-tolerant tree species exposed to fluvial upland systems and wave- or tide-dominated regimes, however, they have encountered severe losses due to sea level rise and anthropogenic activities. Approximately 1.04 million ha of mangrove forests vanished globally between 1990 and 2020 due to sea level rise, deforestation and conversion to agricultural use (Bryan-Brown et al., 2020; Lovelock et al., 2015; FAO, 2020; Fricke et al., 2017). Asia experienced the most severe destruction and a substantial decrease in mangrove forests, with an average annual loss of approximately 1,030 ha in 1990–2000 and a total

loss of 38,200 ha in the most recent decade (Giri et al., 2015; Richards et al., 2015; FAO, 2020). Their valuable ecosystem services such as being ideal ecosystems for nutrient exchange, carbon sequestration, sediment traps, and pollution filters and providing natural habitats for biodiversity are being degraded (Adame and Lovelock, 2011; Brander et al., 2012; Murray, 2012; Lovelock et al., 2017). Therefore, it is necessary to diagnose how and why mangroves have been lost worldwide in the anthropogenic era.

Some studies have demonstrated that sea level rise caused by global warming is a potential threat to mangrove ecosystems (Nicholls and Cazenave, 2010; Kirwan and Megonigal, 2013; Lovelock et al., 2015).

Abbreviations: NRD, Nanliu River Delta.

* Corresponding author at: State Key Laboratory of Estuarine and Coastal Research, East China Normal University, Shanghai, China.

E-mail address: zjdai@sklec.ecnu.edu.cn (Z. Dai).

<https://doi.org/10.1016/j.foreco.2021.119855>

Received 19 August 2021; Received in revised form 28 October 2021; Accepted 2 November 2021

0378-1127/© 2021 Elsevier B.V. All rights reserved.

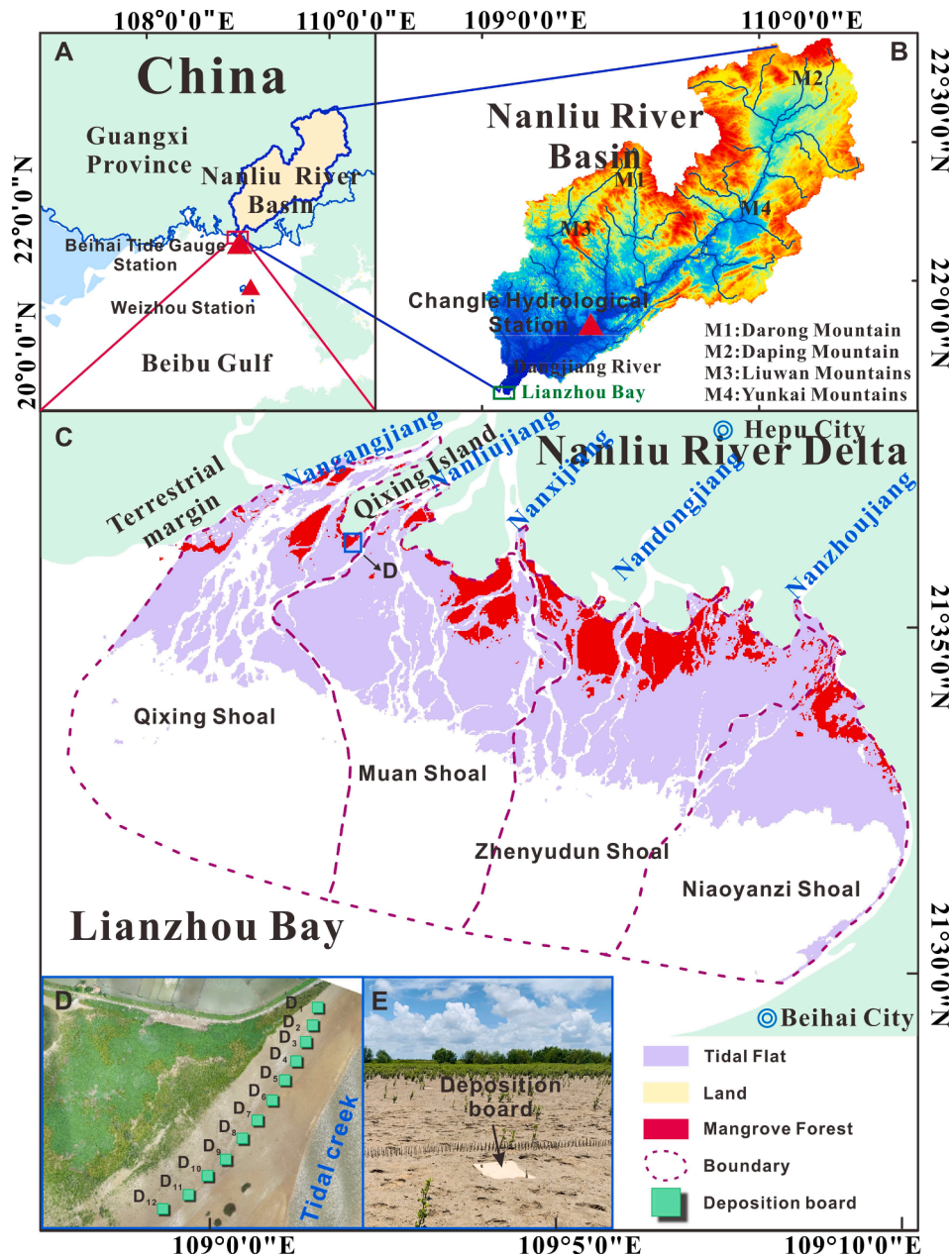


Fig. 1. Research area and general regional features, A: location of the Nanliu River basin and Nanliu River Delta; B: Nanliu River basin and location of the Changle hydrological station; C: study area showing the overall distribution of mangrove forests and tidal flats in the NRD; D: deposition foam board locations; E: deposition board placement.

However, recent work has highlighted that sufficient supply from rivers enables mangrove forests with the capacity to cope with anticipated rising sea levels and maintain their lateral growth (Lovelock et al., 2017; McIvor, 2017; McKee, 2007; Morris, 2002; Woodroffe, 2016). Furthermore, because of globally declining sediment delivery to the ocean due to upstream dam construction (Syvitski et al., 2009), many deltas in tropical regions, such as the Chao Phraya River Delta of Thailand and the Mekong River Delta of Vietnam, sink below local sea level, putting mangrove forests at risk of drowning (Syvitski et al., 2009; Milliman et al., 2011; Hu et al., 2020). However, Long et al. (2021) revealed that when the local suspended sediment concentration of the Red River estuary remained almost unchanged, mangrove forests could maintain seaward horizontal growth (Long et al., 2021), even though fluvial sediment delivered into the delta exhibited decreases (Gao et al., 2015). The drivers of losses or gains of global mangrove forests can be holistically determined by the fluvial suspended sediment discharge supply,

changes in the local suspended sediment concentration, and the relationship between estuarine hydrodynamics and mangrove forest ecosystems.

Hydrodynamics could control the local physical environment and determine the distribution patterns of mangrove forests (Ball, 1988; Berger et al., 2008; Woodroffe et al., 2016; Raw et al., 2019). When tidal flooding carries sediments upstream into the estuary, the exposed aerial root systems of mangrove forests weaken tidal velocity by increasing friction so that the velocity of ebb flows carrying sediments downstream is slowed, and then the sediments are stored and deposited, which is called the “tidal pumping” effect (Furukawa and Wolanski, 1996; Wolanski, 2006; Woodroffe et al., 2016). Sediment deposits can be resuspended by wave action and then delivered to estuaries by tidal currents at flood tide to promote the progradation of mangrove forests in a low wave energy environment (Van Santen et al., 2007; Gedan et al., 2011; Hu et al., 2015; Sánchez-Núñez et al. 2019). When exposed to a

high-wave-energy environment, a large amount of marine sediment may be deposited in the estuary, form barriers and close the inlet. Prolonged closure would intensify the risk of mangrove forests being inundated, which limits them from expanding further (Mbense et al., 2016; Raw et al., 2019). For example, this situation has occurred to mangroves in the Mngazana Estuary of the Eastern Cape, South Africa, and the Ba Lat Estuary of the Red River Delta, Vietnam (Rajkaran et al., 2012; Van Santen et al., 2007; Long et al., 2021).

Moreover, anthropogenic activities are responsible for the majority of mangrove loss (Adame et al., 2018). In deforestation hotspots, such as Malaysia, Myanmar, and Indonesia, most of the lost mangrove forests were converted to aquaculture, rice or oil palm plantations (Adame et al., 2018; Gandhi et al., 2019; Richards et al., 2015). Generally, it takes decades for mangrove forests to grow from the propagule stage to maturity (Hoff et al., 2010). Unfortunately, when their complicated community structure is destroyed by human activities or natural disasters, it is difficult or even impossible for mangrove forests to recover naturally to the original community (Cortina et al., 2006). Therefore, in recent decades, governments and organizations in many nations have made great efforts to plant mangroves in order to reverse the continual degradation of mangrove forests, but these efforts sometimes are not successful below mean sea level, where ecological and hydrological conditions are not suitable for them to grow (Lewis, 2005; Lewis and Brown, 2014; Lewis et al., 2019; Lee et al., 2019). Conversely, this measure has destroyed the structure of the ecosystem and even hastened the demise of mangrove forests because of the lack of sensible recovery policies (Lee et al., 2019). Hence, an urgent requirement for mangrove conservation is a better understanding of the hydrologic and geomorphological requirements of mangroves and their sustainable management.

Monitoring mangrove forests by field observation is inefficient and time-consuming because they are widely distributed and difficult to access. However, in recent decades, the development of accessible remotely sensed data, combined with advanced classification algorithms and available image processing applications, has made it possible to easily map mangrove forests on a large scale (Giri, 2016). Medium-resolution images, such as Landsat Thematic Mapper (TM) and Spot High Resolution Visible (HRV) data, have been widely used for mangrove mapping (Giri et al., 2010; Long et al., 2014; Thomas et al., 2018), and they are acknowledged as the best option for applications on a national or regional scale (Kuenzer et al., 2011; Kirui et al., 2013). Furthermore, even though some studies have described the spatial distribution of mangrove forests worldwide, little information is available regarding mangrove forest spatial variation and associated coastal dynamics forcing, especially those of the Nanliu River Delta (NRD), the largest delta in the northern Beibu Gulf, China. In this study, multiple images from Landsat TM, Enhanced Thematic Mapper Plus (ETM+), Operational Land Imager (OLI), long-term hydrosediment data, and mangrove forest growth observations were collected to profile the dynamic pattern of mangrove forests in the NRD. The main aims of this study were to 1) quantify the aerial area of mangrove forests in the NRD between 1986 and 2020; 2) profile the spatial geomorphological change patterns, and 3) discern the main drivers affecting the losses and gains of mangrove forests in the NRD.

2. Materials and methods

2.1. Study area

Accounting for more than 37% of the total area of mangrove forests in China, mangrove forests in Beibu Gulf constitute the second largest mangrove forest area in China (Jia et al., 2015). The Nanliu River, the largest river in Southwest China, originates from Darong Mountain and Daping Mountain in Guangxi, flows 287 km southward through the Liuwan Mountains and Yunkai Mountains, braids near the Dangjiang River in Hepu city, enters the NRD and discharges into the Beibu Gulf

(Fig. 1) (Tong et al., 2018). It has five tributaries, Nanganjiang, Nanliujiang, Nanxijiang, Nandongjiang and Nanzhoujiang, from west to east (Chen et al., 1988). Controlled by a distinct subtropical monsoon climate, the flood season of the NRD is from May to October, while the dry season is from November to April. The average annual rainfall ranges from 1500 to 1800 mm, and the annual average temperatures are between 21.5 °C and 22.4 °C. Due to the special geographical location and climatic conditions, the NRD experiences frequent typhoons and storm surges, but fertile soil and sufficient heat make it an ideal environment for mangrove growth (Li et al., 2017; Zhao et al., 2017; Wang et al., 2020).

The Nanliu River Delta covers an area of 550 km² and is the largest delta in Beibu Gulf. The average annual water discharge and annual total suspended sediment at the Changle gauging station, the tidal limit of the delta, were reported to be $1.9 \times 10^{12} \text{ m}^3 \text{ y}^{-1}$ and $350 \times 10^6 \text{ t y}^{-1}$, respectively (Li et al., 2017; Tang et al., 2021). Dense mangroves including *Aegiceras corniculatum*, *Kandelia candel*, *Avicennia marina*, *Excoecaria agallocha* and *Sonneratia apetala* grow at the edge of the ocean. Outside the entrance of the Nanliu River is Lianzhou Bay, approximately 14 ~ 18 km long from east to west and 15 km wide from north to south (Fig. 1) (Yang et al., 1995; Chen et al., 1997). The northern, eastern, and southeastern parts are surrounded by continents, which are shaped like semi-arcs facing southwest and connected to Beibu Gulf (Fig. 1B and 1C). Extensive shallow tidal flats, most of which are below 5 m, are well developed in the northern and western bays, accounting for 80% of the total area of the NRD (Luo et al., 1992; Chen et al., 2007). These mangrove forests of the NRD are divided into four regions, referred to as Qingxing Shoal, Muan Shoal, Zhenyudun Shoal, and Niaoyanzi Shoal. Furthermore, the mangrove forests of the NRD are composed of western and eastern parts that are isolated from the Nanxijiang River (Fig. 1), where Qixing Shoal and Muan Shoal belong to the western part, and Zhenyudun Shoal and Niaoyanzi Shoal belong to the eastern part.

The NRD is a tide-dominated delta subject to strong tidal action, and freshwater inputs are not abundant compared with those of other large river deltas, such as the Yangtze River Delta (Dai et al., 2018; Song et al., 2012; Li et al., 2017). Wind-driven waves are the most typical wave in Lianzhou Bay and are driven by the southwestern summer monsoon. Wave action is relatively weak, with a mean wave height of approximately 0.3 m, and the seasonal wave climate is obvious, with southwestern (SW) waves in summer and north-northeastern (NNE) waves in winter (Chen, 1997; Chen, et al., 1988). Lianzhou Bay is characterized by irregular diurnal tides with a mean tidal range of 2.45 m and maximum range of 5.87 m (Chen et al., 1988; Li et al., 2001). The ebb tide velocity in Lianzhou Bay is 104 cm/s, and the flood tide velocity is 88 cm/s (Chen, 1996).

2.2. Materials

Google Earth Engine (GEE) (<https://earthengine.google.com>) is a planetary-scale platform for geospatial data analysis, combining a multi-petabyte catalog of satellite imagery including Landsat surface reflectance data processed by the United States Geological Survey (USGS) (<https://earthexplorer.usgs.gov>). Multiple remote sensing images (path 125 row 45) from Landsat 5 TM, Landsat 7 ETM+ and Landsat 8 OLI are the major materials for mapping the spatial distribution of mangrove forests and tidal flats. A total of 147 cloudless images were selected for processing based on the World Geodetic System 1984 (WGS84) (National Geospatial-Intelligence Agency) geographical coordinate system and Universal Transverse Mercator (UTM) projection coordinate system. However, there were no cloud-free images obtained by Landsat in several years, including 1997, 1995, and 2013. Moreover, images obtained on December 21, 1996, September 1, 2008 and September 18, 2020 were selected to retrieve the distribution of bare tidal flats in the NRD.

The measured tidal levels at the Beihai tidal gauge station

Table 1
Spectral indices used for classification.

| Name | Equation | References |
|---|--|----------------------|
| 1 Normalized Difference Vegetation Index (NDVI) | $NDVI = \frac{(\rho_{nir} - \rho_{red})}{(\rho_{nir} + \rho_{red})}$ | Rouse et al., 1974 |
| 2 Enhanced Vegetation Index (EVI) | $EVI = 2.5 \times \frac{(\rho_{nir} - \rho_{red})}{\rho_{nir} + 6\rho_{red} - 7.5\rho_{blue} + 1}$ | Huete et al., 2002 |
| 3 Mangrove Vegetation Index (MVI) | $MVI = \frac{(\rho_{swir} - \rho_{green})}{(\rho_{swir} + \rho_{green})}$ | Baloloy et al., 2020 |
| 4 Normalized Difference Water Index (NDWI) | $NDWI = \frac{(\rho_{green} - \rho_{nir})}{(\rho_{green} + \rho_{nir})}$ | Gao et al., 1996 |

corresponding to each remote sensing image acquisition time were also taken from the South China Sea Information Center of the State Oceanic Administration. Significant wave height ($H_{1/10}$) data from 1973 to 1995 at the Weizhou ocean monitoring station were used to analyze the hydrodynamics of Lianzhou Bay in Beibu Gulf, and these data were acquired from Huang et al. (2021) (Fig. 1A). Additionally, sedimentation plate experiments implemented from October 2, 2019, to October 7, 2020, were used to analyze erosion/accretion in tidal flats of the NRD (Fig. 1D, 1E). Daily water discharge and sediment load (1965–2020) at the Changle hydrologic station, which is located downstream of the Nanliu River, were obtained from the Guangxi River Sediment Bulletin.

2.3. Methods

2.3.1. Image processing

We used the USGS Landsat Surface Reflectance products, which are atmospherically corrected, to retrieve the distribution of mangrove forests and tidal flats based on the GEE platform (Chen et al., 2017; Deng et al., 2019; Wang et al., 2020). We used “random forest”, which is a computationally efficient and highly effective supervised learning algorithm. The reflectances of blue, green, red, near infrared, shortwave infrared and brightness temperature were selected, and four spectral indices (Table 1) were calculated for each image, serving as inputs for the random forest classifier. Thereafter, the prepared images were classified as mangrove forests, tidal flats, water, and other. The producer accuracy and user accuracy of every classification result exceeded 87% and 89%, respectively.

2.3.2. Spatial analysis of mangrove forests and tidal flats

ArcGIS software is a useful tool for analyzing the spatial variation in ground objects, making supporting geometric calculations, conducting spatial overlay analysis and conducting data visualization (ESRI, 2011). The erase function in the overlay toolset was used to calculate the losses and gains in mangrove forests and tidal flats to discern the change process of mangrove forests (Scott et al., 2010). The shorelines in tidal flats near the low tidal level of approximately 160 cm were extracted by ArcMap to illustrate the progradation of tidal flats every 12 years, i.e., in 1996, 2008 and 2020.

Generally, the centroid is the point corresponding to the geometric center of a polygon or multiple polygons representing a portion of the image. In this study, the centroids of mangrove patches in each year were generated based on ArcGIS software to detect the spatial migration of mangroves, thus quantitatively analyzing the spatial distribution of mangroves and the difference between the eastern and western NRD. To calculate the location of a centroid, assume there is a complicated figure Z. Then the figure Z will be decomposed into simple geometric figures. Given an image Z, obtain the centroid C_i and area A_i of each Z_n part wherein all holes that extend outside the compound shape are treated as negative values. Last, the computation formulas are as follows:

$$C_x = \frac{\sum_{i=1}^n C_{ix} A_{ix}}{\sum_{i=1}^n A_{ix}} \quad (1)$$

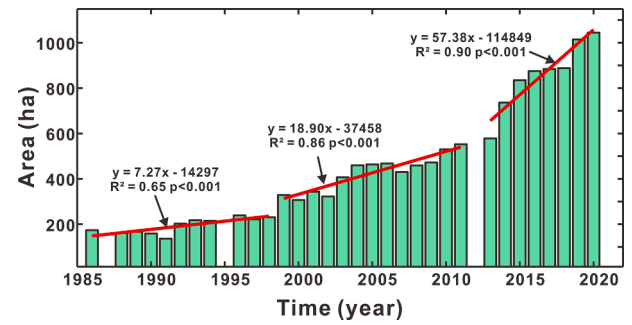


Fig. 2. Changes in mangrove forest area in the NRD from 1986 to 2020.

$$C_y = \frac{\sum_{i=1}^n C_{iy} A_{iy}}{\sum_{i=1}^n A_{iy}} \quad (2)$$

To better distinguish the spatial movement of the centroid of mangrove forests in the past 35 years, the average centroid was calculated every five years in each region and the entire delta.

2.3.3. Sediment deposition measurement

Sedimentation levels were observed for one year from October 2, 2019, to October 7, 2020, using foam boards placed in the middle intertidal zone (Fig. 1D, 1E). A total of 12 deposition foam boards were placed in front of Qixing Island and are presented as D_n ($n = 1, 2, 3, \dots, n$). D_1 represents the sediment deposited in the intertidal zone in November, and D_2 represents the sediment deposited in the intertidal zone in November and December. D_n is the accumulated sediment deposition in the previous n months. Due to the influence of COVID-19, D_4 was not collected. Additionally, 5 500-cm³ soil samples were randomly selected from the intertidal zone where the foam boards were located. After the collected sediment was dried and weighed, its mean dry weight ρ was 1368.6 kg. Based on this result, the monthly accumulated sediment on each board collected after drying and weighing and then dividing by ρ , namely, the monthly accumulated sediment height H of the tidal flat, was obtained.

3. Results

3.1. Changes in mangrove forests areas

3.1.1. Changes in the total area

Trend analysis segmented into three periods of mangrove forest area time series between 1986 and 2020 exhibited marked upward trends, which ranged from 173.5 ha in 1986 to 1044.4 ha in 2020 (Fig. 2), an expansion of approximately 5 times (Fig. 2). Specifically, the mangrove forest areas of the NRD increased at a rate of 7.3 ha/y between 1986 and 1998 but these forests increased more quickly at a rate of 18.9 ha/y between 1999 and 2011. The sharpest increase in mangrove forests ranged from 578.4 ha in 2013 to 1044.4 ha in 2020. However, mangrove forests in distinct territories of the NRD increased at different rates (Figs. 1 and 3).

3.1.2. Area changes in different regions

The area of mangrove forests in Qixing Shoal first dramatically declined between 1986 and 1998 and then rapidly increased between 1999 and 2020 (Fig. 3A). In particular, a turning point was observed in 1998 with a decreased rate of 6.83 ha/y and an increase rate of 4.32 ha/y before and after 1998, respectively (Fig. 3A). Meanwhile, the mangrove forests in Muan Shoal, Zhenyudun Shoal, and Niaoyanzi Shoal mostly increased at steady rates of 3.6 ha/y, 8.6 ha/y, and 3.23 ha/y between 1986 and 1998, respectively. However, after 1998, the expansion rate of mangrove forests in Muan Shoal and Zhenyudun Shoal accelerated to 3.9 ha/y and 10.8 ha/y (Fig. 3A, 3B, 3C), respectively.

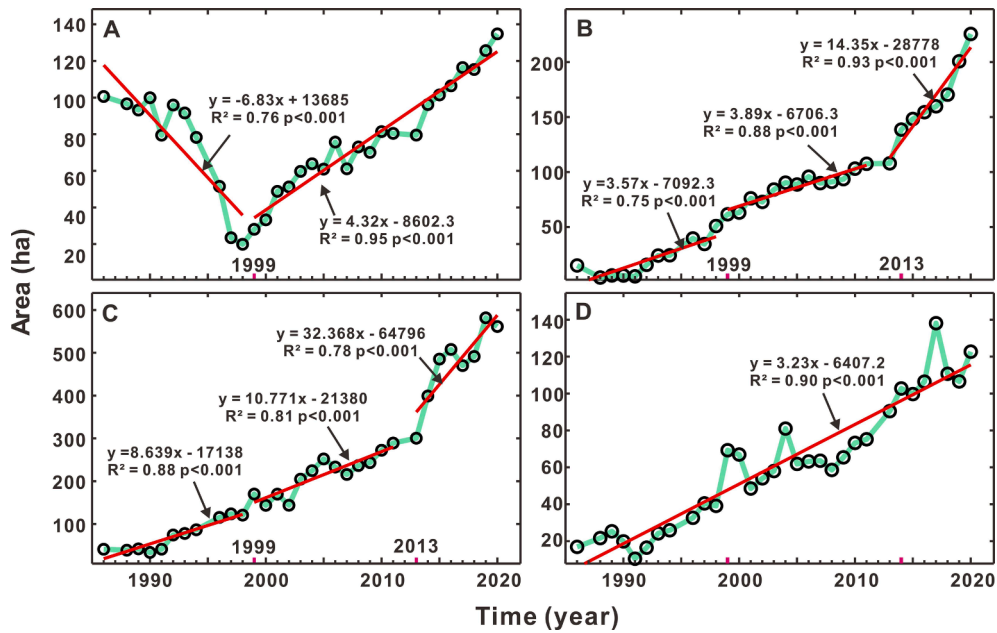


Fig. 3. Temporal changes in mangrove forest area in each region.

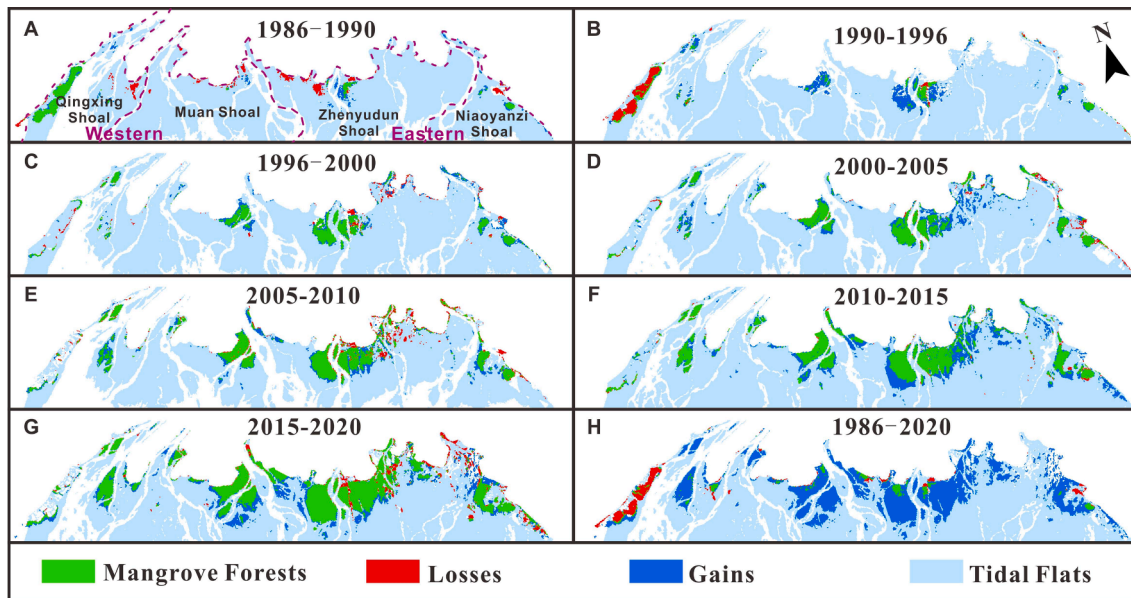


Fig. 4. Variation in mangrove forest spatial distribution in the NRD.

Furthermore, the change rates from 2013 to 2020 of Muan Shoal and Zhenyudun Shoal suddenly skyrocketed to 14.4 ha/y and 32.4 ha/y (Fig. 3B, 3C), respectively, even though the mangrove forests in Niaoyanzi Shoal maintained a constant rate in the past three decades (Fig. 3D).

The majority of mangrove forests were distributed in Qixing Shoal in 1986, which accounted for 58% of all mangrove forests (Fig. 3). However, the mangrove forests in Qixing Shoal experienced a drastic reduction between 1986 and 1998 (Figs. 1 and 3A), and the total percentage of the other three deltaic shoals increased from 42% in 1986 to 91% in 1998 (Fig. 3A-D). Then, after 1998, although the mangrove forests in Qixing Shoal began to recover with approximately 13% of the deltaic mangrove forests showing increases, those in Muan and Zhenyudun Shoals apparently increased to 22% and 54%, respectively (Fig. 3A, 3B, 3C). The mangrove forest in Niaoyanzi Shoal was

approximately 15 times that of Qixing Shoal, which accounted for 60% of the total mangrove forest area (Fig. 3).

3.2. Spatial patterns of mangrove forests

Although the area of the deltaic mangrove forests presented an upward trend (Fig. 2), the spatial expansion of mangrove forests was not synchronized (Fig. 4). Specifically, between 1986 and 1990, a clear mangrove forest belt grew along the terrestrial edge in the western Qixing Shoal with a length of 2.6 km and width of 500 m, and some small patches of mangrove forests were scattered over the deltaic shoals and several central riverine islands (Fig. 4A). Mangrove forest losses occurred along the coast on southern Qixing Island, in Muan Shoal and in the western Zhenyudun Shoal, while major gains were concentrated on central Niaoyanzi Shoal (Fig. 4A). However, between 1990 and

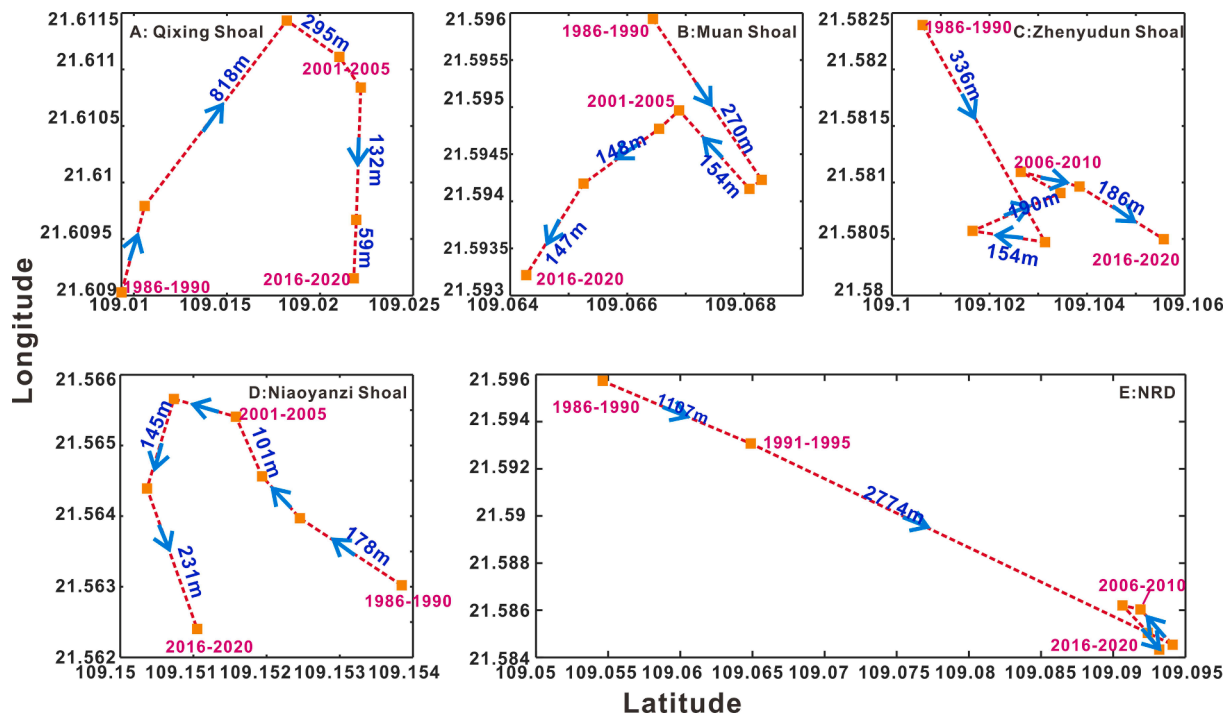


Fig. 5. Spatial movement of area-weighted centroids of mangrove forests.

1996, the preexisting mangrove forest belt along the terrestrial edge of the NRD completely disappeared (Fig. 4B). Gains of mangrove forests occurred on the outside edges of Qixing and Muan Shoals. Meanwhile, the scattered mangrove forest patches migrated toward the southeast (Fig. 4B). Between 1996 and 2005, previously gained mangrove forest patches slowly expanded to the southeast along Muan Shoal and Niaoyanzi Shoal, and the mangrove forests in Zhenyudun Shoal increased suddenly between 2000 and 2005 in comparison with those between 1996 and 2000 (Fig. 4C, 4D). Between 2005 and 2010, except for the extensive losses in Zhenyudun Shoal, the mangrove forests in other regions all presented net gains (Fig. 4E). Between 2010 and 2020, net increases in mangrove forests occurred on the outer edges of mangrove forests of the whole NRD (Fig. 4F, 4G). Between 1986 and 2020, the mangrove forests at the terrestrial edge of the NRD were permanently damaged, and although sporadic losses and gains occurred in other regions, they all eventually presented net gains (Fig. 4H).

3.3. Transfer of the centroid in mangrove forests

The centroid of mangrove forests in Qixing Shoal showed long-distance migration, approximately 4393 m from southwest to southeast between 1986 and 2020 (Fig. 5A). Large shifts occurred between 1991 and 1995, with northeastward movement of 818 m and southwestward movement of 132 m between 2006 and 2010 (Fig. 5A). Meanwhile, the centroid of mangrove forests in Muan Shoal migrated 270 m southeastward during 1986–1990 and then shifted to the southwest in 2000 with continuous seaward expansion (Fig. 5B). The centroids of the mangrove forests in Zhenyudun Shoal were colonized by mangroves in the southeast except that they shifted to the northwest between 1991 and 1995 and then shifted to the northeast during 1996–2000 (Fig. 5C). A similar movement pattern was observed in Qixing Shoal near Niaoyanzi Shoal; the centroid moved to the northwest between 1986 and 2005 and subsequently migrated to the southwest (Fig. 5D). The centroid in the western part (Qixing Shoal and Muan

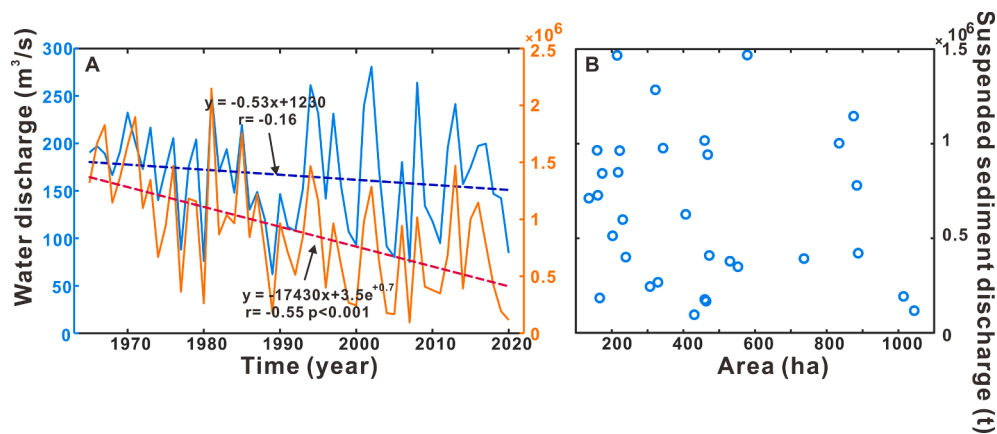


Fig. 6. A: Average annual water discharge and suspended sediment discharge at Changle station from 1965 to 2020 and their simple linear regression analysis (water discharge shown by the blue dashed line, suspended sediment discharge shown by the red dashed line). B: Relationship between the area of mangrove forests and suspended sediment discharge. (For interpretation of the references to colour in this figure legend, the reader is referred to the web version of this article.)

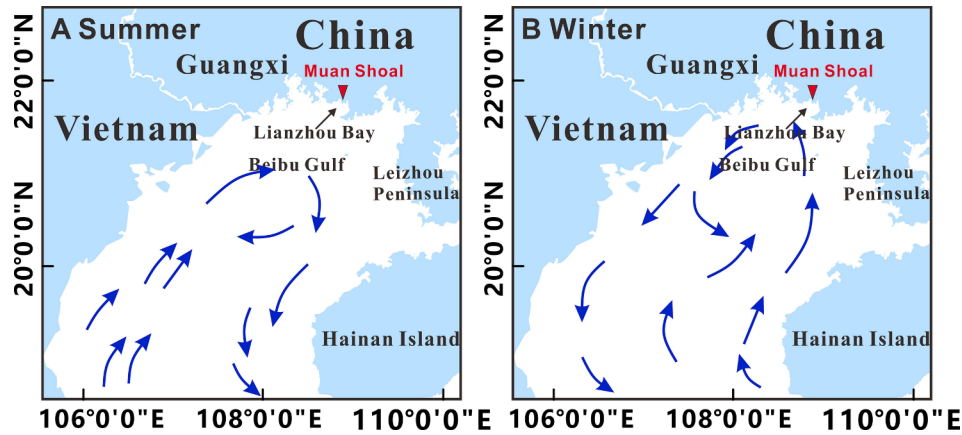


Fig. 7. Tidal current flow in Beibu Gulf in summer and winter.

Shoal) finally moved to the southwest, while the centroid in the eastern part (Zhenyudun and Niaoyanzi Shoals) shifted to the southwest (Fig. 5A, 5B, 5C, 5D). Generally, the centroid of mangrove forests in the NRD migrated approximately 4000 m from northwest to southeast during the study period (Fig. 5E).

4. Discussion

4.1. Impacts from suspended sediment discharge upstream

Sediment transport by estuarine rivers can promote the progradation of deltaic tidal flats and create new physical space for mangrove forest growth (Swales et al., 2019). Some studies have indicated that a reduction in riverine suspended sediment discharge will slow the expansion rate of deltaic mangrove forests or lead to the loss of mangrove forests (Lovelock et al., 2021; Worthington et al., 2020). Here, based on water discharge and suspended sediment discharge analyses of the Changle hydrological station between 1965 and 2020, the water discharge level did not change, but the sediment load declined dramatically by approximately 1.2 tons over the same period (Fig. 6A). More specifically, the suspended sediment contribution from the Nanliu River to Lianzhou Bay indicated a decrease of 726 thousand tons during the last 35 years from 1986 to 2020, while the annual change in mangrove forest area showed no response to such large fluvial sediment variation, which means that the declining sediment transported to the delta mouth did not directly affect the expansion of mangrove forests (Fig. 6B). In other words, the expansion of the mangrove forest area in the NRD could be controlled by other factors.

4.2. Estuarine sediment dynamics

4.2.1. Suspended sediment transport induced by tidal currents

Previous studies indicated that the NRD is a tide-dominated delta with a mean tidal range of 2.54 m (Chen 1988; Jiang et al., 2008). Wind is the main forcing that triggers changes in tidal currents in the adjacent ocean areas of the delta (Chen 1988; Yang et al., 1995). In summer, the wind-driven currents flow clockwise around Beibu Gulf under the influence of the southwestern monsoon (Fig. 7A), the western waters of the Nanliu River Estuary are dominated by flood tide, and the eastern waters are controlled by ebb tide (Fig. 7A). The maximum residual current velocity resulting from wind-sea currents can reach 29.3 cm/s (Chen Bo, 1996). Therefore, suspended sediment brought from the northeastern flood tide is transported from the southwest to northeast and then settles in Muan Shoal—the eastern delta. Meanwhile, Zhenyudun Shoal is sheltered by Beihai Peninsula (Fig. 1A, 1C), where there are large-scale depositions due to gradual sediment deposition induced by the southeastward ebb tide, thus enhancing the expansion of Zhenyudun Shoal (Fig. 7A). In the winter, northerly and easterly winds dominate with counterclockwise wind currents (Fig. 7B) formed in this area. Sediments carried by the flood tide are delivered from the southeast to northwest and are then transferred to the southwest near Muan Shoal; thus, delta shoals in the east of Muan Shoal are still building. Muan Shoal is just in the buffer zone of the southwestern ebb tide current and discharges from the western Nanliu River mainstream (Figs. 1, 7); therefore, sediments were deposited over the shoals in the southwestern direction due to the influence of the winter southwest ebb tide. Consequently, the tidal flats of the delta are deposited under the

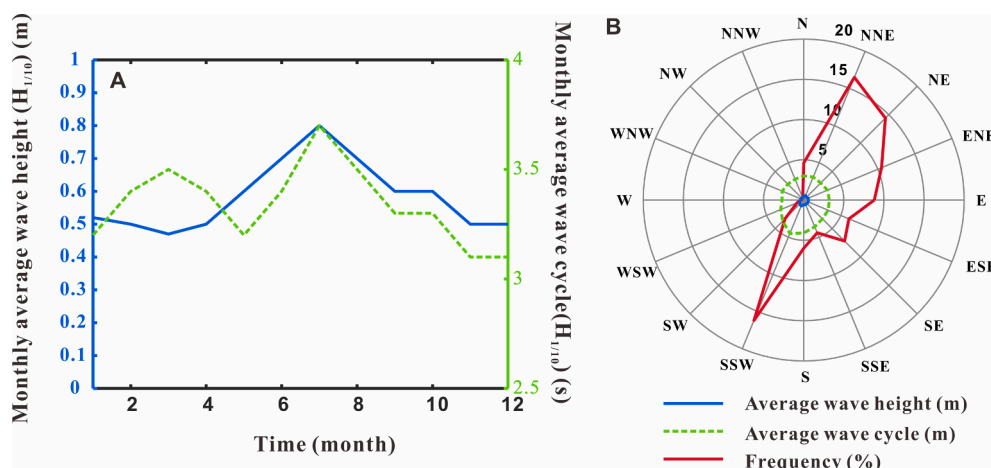


Fig. 8. Characteristics of waves at Weizhou station. A: Monthly significant wave height ($H_{1/10}$). B: Direction of waves at Weizhou station.

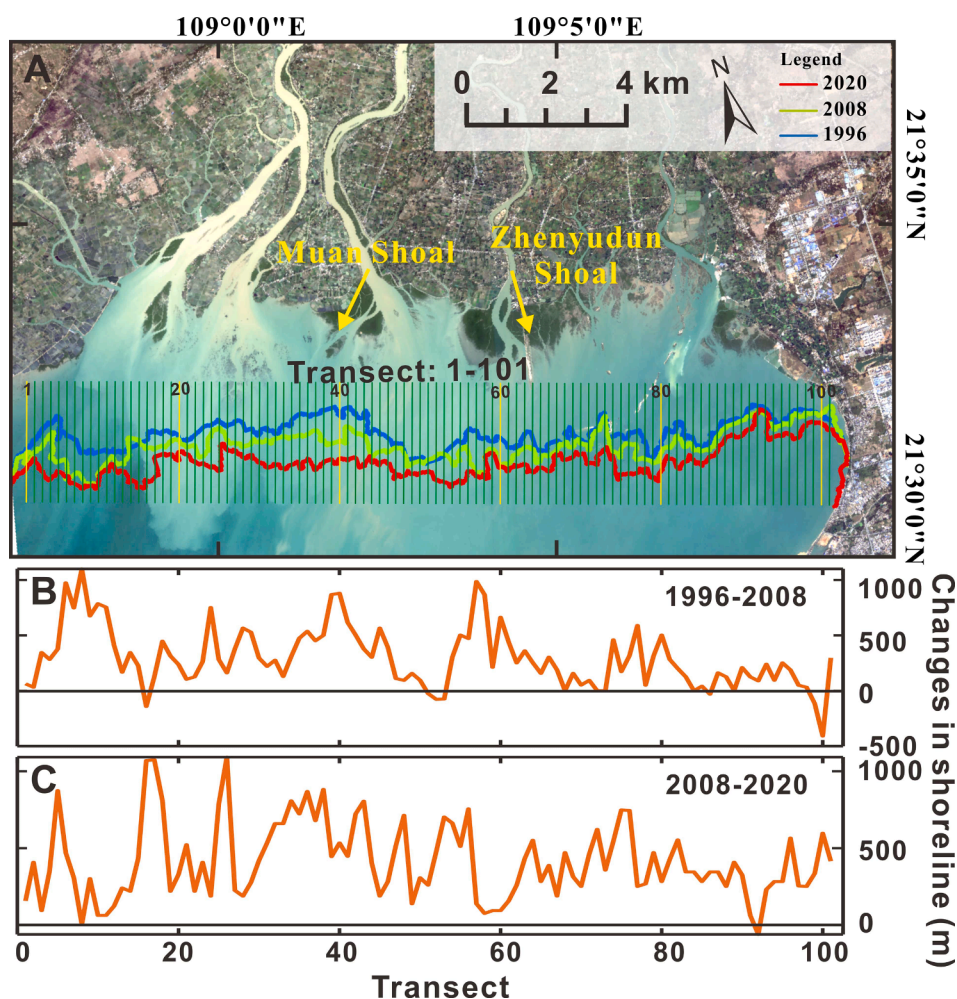


Fig. 9. Shorelines of bare tidal flats in the NRD. A: The blue, green, red lines represent the shorelines in 1996, 2008 and 2020, respectively; B: progradation and erosion of shoreline during 1996–2008 and 2008–2020, respectively, where positive represents progradation and negative represents erosion. (For interpretation of the references to colour in this figure legend, the reader is referred to the web version of this article.)

influence of sediment inputs from the wind-driven currents in winter and summer, which provide space for mangrove forests to expand toward the sea (Fig. 7).

4.2.2. Wave action

Lianzhou Bay is dominated by southwestern waves with a mean height of 0.3 m in summer, and winter is characterized by northeastern waves with a mean height of 0.48 m (Chen, 1988) (Fig. 8). Additionally, weak wave heights have difficulty generating large wave currents to transport sediment, regardless of the wave direction, i.e., southwestward or northward waves. However, when water is at a relatively low level, the southwestward waves could easily resuspend fine particles, which could then be redeposited on the southeast deltaic shoal (Fig. 7). While the northeastward waves are weaker and can also resuspend fine sediments, the tidal tides deliver the sediments southwestward to the mangrove forest habitat and offshore area. Therefore, the delta shoal controlled by southwestward waves is basically oriented to the southeast, and it is dominated by clayey silt, with a small amount of sand (Wang, 2021). It can largely promote the migration of the mangrove forest centroid to migrate to the southeast (Fig. 5). Meanwhile, oriented from the western to eastern NRD, the wave action is sheltered by the eastern Beihai Peninsula and significantly smaller in the eastern part than in the western part; additionally, the expansion of mangrove forests in areas with relatively weak dynamic conditions is faster than that in other areas (Fig. 4). In brief, although wave action has little effect on suspended sediment transport, waves can resuspend sediments in the

shoal and increase the suspended sediment concentration in the water, thus playing an auxiliary role in sediment transport to the tidal flats of the delta. Moreover, the mangrove forests in the NRD grow in a low wave energy environment, which is dominated by southwestern waves; therefore, most mangrove forests in the NRD shifted from the southwest with expansion to the southeast (Gedan et al., 2011; Sánchez-Núñez et al. 2019; Long et al., 2021).

4.3. Impacts of bare tidal flats

Mangrove forests often occur in the tidal flats of deltas, but they can survive only on tidal flats that are slightly above mean sea level (Krauss et al., 2014; Xiong et al., 2021). Here, under three identical low tide levels between 1996 and 2008, the shorelines of tidal flats were broadly deposited into the sea, especially for transects 6–12, 34–46, and 54–67, which expanded at rapid rates of 65 m/y, 43 m/y, and 35 m/y, respectively, and they corresponded to the positions of the deltaic area of the Nanliu River main stream, Muan Shoal and Zhenyudun Shoal, respectively (Fig. 9A, 9B, 9C). Between 2008 and 2020, significant expansion occurred along transects 16–26, 30–48, 52–56, and 72–78 of the four shoals with rates of 51 m/y, 49 m/y, 51 m/y, and 40 m/y, respectively (Fig. 9A, 9B, 9C). When the bare tidal flats of the NRD expanded significantly to the sea (Fig. 9B, 9C), extensive losses occurred in the back margin of the bare tidal flats, which were occupied by the newly expanded mangrove forests (Fig. 10A, 10B, 10C), resulting in the essentially unchanged area of bare tidal flats from 1996 to 2020

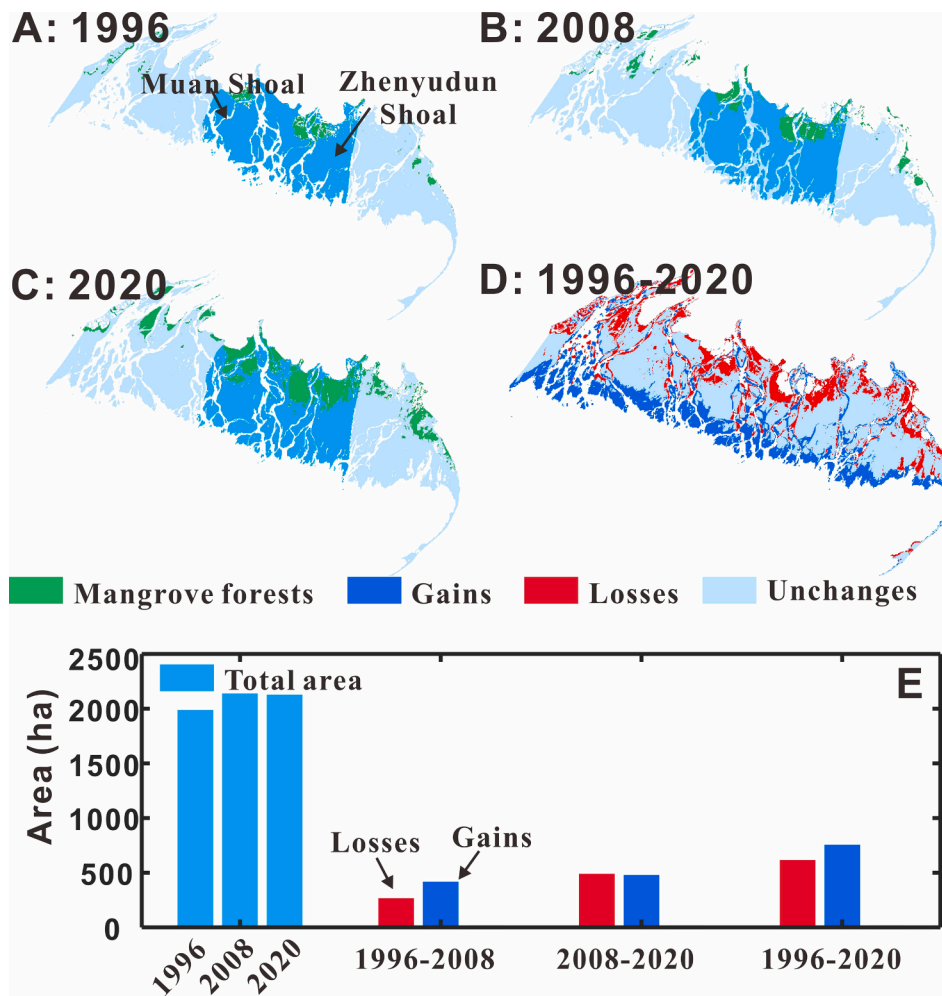


Fig. 10. Variation in the spatial distribution of tidal flats. A-C: Spatial distribution of bare tidal flats and mangrove forests in 1996, 2008, 2020, respectively; D: total losses and gains of bare tidal flats during the period of 1996–2020; E: area of bare tidal flat in front of mangrove forests in Muan Shoal and Zhenyudun Shoal and loss and gain areas of the three periods.

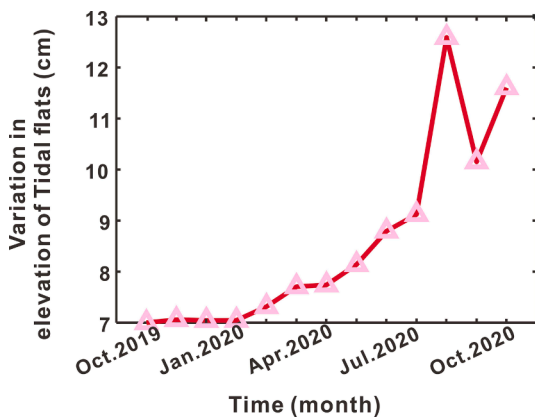


Fig. 11. Vertical change in tidal flats from October 2, 2019, to October 7, 2020.

(Fig. 10D, 10E).

Furthermore, a one-year deposition experiment in the Nanliu Estuary illustrated that the annual accretion rate of tidal flats was 0.046 m/y (Fig. 11). This result means that bare tidal flats expanded laterally toward the sea; at the same time, they accreted vertically to increase in elevation, thereby forming tidal flats that were conducive to the establishment of mangrove forests. For example, around Qingxing Island, in

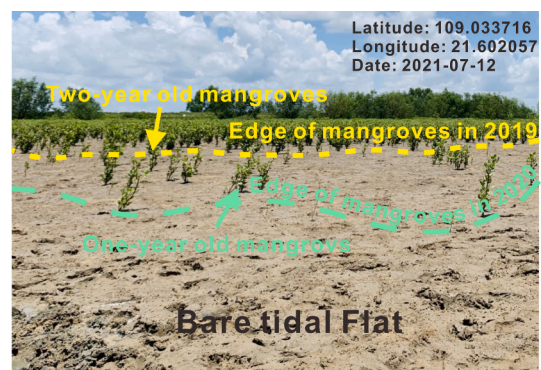


Fig. 12. The process of mangrove forest expansion in bare tidal flats.

2019, some annual *Aegiceras corniculatum* grew in tidal flats with elevations of 0.12 m above mean sea level (Fig. 12). Then, in 2021, the one-year-old mangrove saplings became two-year-old mangrove saplings, and a new one-year-old *Aegiceras corniculatum* was established approximately 5 m from the two-year old mangrove saplings toward the sea (Fig. 12). Apparently, when local dynamic conditions remain unchanged, the lateral expansion and vertical accretion of bare tidal flats can provide a suitable physical environment for mangrove forest growth. After mangroves are established, they can rapidly capture

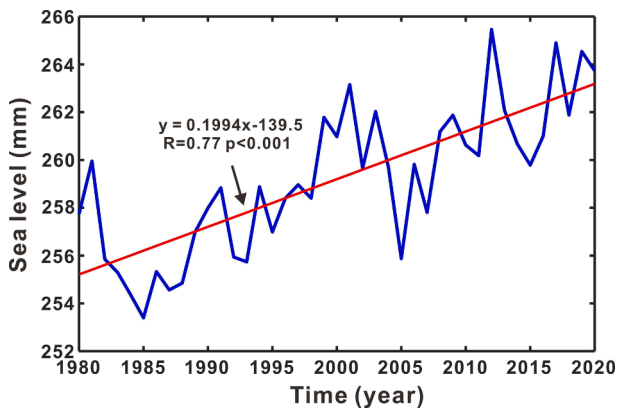


Fig. 13. The mean sea level at Beihai station from 1980 to 2020.

sediment and result in further deposition in adjacent areas, which helps more mangrove forests migrate to the bare flats (Fig. 12). Bare tidal flats with adaptable elevations provide necessary living space for mangrove forests, which is probably an important factor coupling tidal flat extension and mangrove forest colonization in the NRD (Swales and Bentley, 2008; Wang et al., 2021).

4.4. Sea level rise

Some studies have noted that sea level rise has directly resulted in a loss of mangrove forests (Lovell et al., 2015; Lovell et al., 2017). The NRD is located in the inner part of Beibu Gulf, and the sea level of the delta increased from 1986 to 2020, with an annual average rate of

0.2 mm per year (Fig. 13). However, the mangrove forests in the NRD colonized toward the sea constantly in this period, which means that sea level probably does not currently affect the seaward expansion of mangrove forests. The annual change in elevation measured in the study area was 0.046 m per year (Fig. 11), which was higher than the current rate of sea level rise. Therefore, considering that there is a wide range of tidal flats outside the mouth of the Nanliu River Delta, the local suspended sediment caused by waves can still be transported into the tidal flats by regional tidal currents, promoting vertical elevation gains and lateral extension of the tidal flats. Meanwhile, subsurface processes beneath organic-rich mangroves mudflats such as root growth and decomposition, endow mangroves with significant elevation (Lovell et al., 2017; Webb et al., 2013; Woodroffe et al., 2016; Woodroffe, 1995). Consequently, both vertical aggradation of inorganic sediment and sequestration of organic matter reduce the stress of being inundated due to sea level rise (McLvor et al., 2013; Woodroffe et al., 2016; Long et al., 2021).

4.5. Human interferences

Globally, large scale loss of mangrove forests has occurred because of deforestation, aquaculture and rice agriculture (Hamilton, 2013; Thomas et al., 2018). In 1992–1998, approximately 95 ha of mangrove forests along the western terrestrial margin of the Nanliu Delta disappeared due to dike and aquacultural pond construction, which induced an abrupt turning point for mangrove forest variation in 1998 (Fig. 3A, 14A, 14B, 14C). In 1985–2020, sporadic tidal flat losses along the bank were attributed to the breeding of sea ducks that occupied the space of mangrove forests (Fig. 4C, 4E, 4H, 14D, 14E). However, with the establishment of the mangrove nature reserve and increased



Fig. 14. Influence of human activities on mangrove forests in the NRD. A: deforestation along the sea wall by local residents; B: conversion of mangrove forests into aquaculture ponds; C: harbors near mangrove forests; D and E: sea duck breeding in mangrove forests; F and G: *Kandelia candel* transplanted by the local government.

mangrove protection, the government prohibited the destruction of mangrove forests, and a wide range of mangrove restoration policies were implemented, facilitating substantial growth of mangrove forests in Muan Shoal and Zhenyudun Shoal in the last decade (Fig. 3B, 3C, 4F, 4G). Thereafter, the mangrove forests in Zhenyudun Shoal were lost again, probably because mangrove forests are usually re-established in intertidal mud-flats below mean sea level, which cannot satisfy the ecological requirements of mangroves (Lewis, 2005; Lewis and Brown, 2014).

However, during 2013–2020 in Zhenyudun Shoal, there was a sudden, substantial increase in the aerial extent of mangroves, which was related to the mangrove restoration carried out by the local government in approximately 2012 (Fig. 14F, 14G). The loss of mangrove forest in Zhenyudun and Niaoyanzi Shoals was likely due to flooding of the tidal flats following elevation decline. It can be concluded that large-scale transplanting leads to a sharp increase in mangrove forests, while wide land use conversion of mangrove forests yields substantial loss of mangrove forests.

5. Conclusions

Accounting for more than 37% of the total area of mangrove forest in China, the mangrove forests in Beibu Gulf constitute the second largest mangrove forest area in China. Here, we explored the dynamic changes in mangrove forests of the largest delta in Beibu Gulf between 1986 and 2020 and clarified the possible reason for mangrove forest variations and conversions. The main findings are as follows:

1. The total area of mangrove forests in the NRD increased incrementally between 1986 and 2020. While a rapid drop and increase on mangrove forests occurred in the western side of the delta before and after 1998, respectively, the mangrove forests in the eastern part increased at a steady rate. Additionally, most mangrove forests in the NRD expanded to the southeast in 1986–2020 due to the limitation of the southwestward advance for barrier effects from southwestward wave action.
2. Sediments carried by tidal currents in estuaries support the expansion of mangrove forests. Wave action triggers resuspension of sediments in the shoals and to increases their concentration in water, which greatly enhances the amounts of sediments transported by tidal currents. The horizontal seaward progradation and vertical accretion of bare tidal flats in the NRD provided tidal flats for seaward mangrove forest expansion.
3. Sea level rise and declining sediment supply had little impact on the seaward expansion of mangrove forests in the NRD, whereas human activities caused a sudden substantial decrease (1992–1998) and increase (2013–2020) in mangrove forests. Converted aquacultural ponds and the behavior of sea ducks along banks were the main reasons for the large losses, while the implementation of mangrove restoration policies by the government has led to the rapid growth of mangrove forests in recent years.

Credit authorship contribution statement

Chuqi Long: Methodology, Software, Visualization, Data curation, Writing – original draft. **Zhijun Dai:** Conceptualization, Methodology, and paper revision. **Riming Wang:** Validation. **Yaying Lou:** Validation. **Xiaoyan Zhou:** Partly calculation. **Shushi Li:** Investigation. **Yuhua Nie:** Investigation.

Declaration of Competing Interest

The authors declare that they have no known competing financial interests or personal relationships that could have appeared to influence the work reported in this paper.

Acknowledgments

This research was supported by the National Natural Science Key Foundation of China (41930537) and Key Projects of Science and Technology of Guangxi Province (AB21076016). We acknowledge Editor Cindy Prescott and two anonymous reviewers for their constructive suggestions to improve previous version of the manuscript.

References

- Adame, M.F., Lovelock, C.E., 2011. Carbon and nutrient exchange of mangrove forests with the coastal ocean. *Hydrobiologia* 663 (1), 23–50.
- Adame, M.F., Brown, C.J., Bejarano, M., Herrera-Silveira, J.A., Ezcurra, P., Kauffman, J. B., Birdsey, R., 2018. The undervalued contribution of mangrove protection in Mexico to carbon emission targets. *Conserv. Lett.* 11 (4), e12445.
- Ball, M.C., 1988. Ecophysiology of mangroves. *Trees* 2 (3), 129–142.
- Baloloy, A.B., Blanco, A.C., Raymund Rhommel, R.R.C., Nadaoka, K., 2020. Development and application of a new mangrove vegetation index (MVI) for rapid and accurate mangrove mapping. *ISPRS J. Photogramm. Remote Sens.* 166, 95–117.
- Berger, U., Rivera-Monroy, V.H., Doyle, T.W., Dahdouh-Guebas, F., Duke, N.C., Fontalvo-Herazo, M.L., Hildenbrandt, H., Koedam, N., Mehlig, U., Piou, C., Twilley, R.R., 2008. Advances and limitations of individual-based models to analyze and predict dynamics of mangrove forests: A review. *Aquat. Bot.* 89 (2), 260–274.
- Brander, L.M., Wagtendonk, A.J., Hussain, S.S., McVittie, A., Ploeg, S., 2012. Ecosystem service values for mangroves in Southeast Asia: a meta-analysis and value transfer application. *Ecosyst. Serv.* 1 (1), 62–69.
- Bryan-Brown, D.N., Connolly, R.M., Richards, D.R., Adame, F., Friess, D.A., Brown, C.J., 2020. Global trends in mangrove forest fragmentation. *Sci. Rep.* 10, 7117.
- Chen, B., 1988. Preliminary analysis of features of hydrodynamic in Lian Zhou Bay. *Coast. Eng.* 7 (3), 33–38.
- Chen, B., 1996. Preliminary Analysis of the Characteristics of the Tidal and Residual Currents in Lianzhou Bay. *Guangxi Science* 3(4), 18–21,37.
- Chen, B., 1997. Marine environmental characteristics of Nanliu River Delta, Guangxi. *Guangxi Sciences*, 3(1):1 8-21, 37.
- Chen, B., Qiu, S.F., Liang, W., 2007. Analysis on Formation of Underwater Delta Shoal and Tidal Groove of Lianzhou Gulf Nanliujiang River. *J. Guangxi Acad. Sci.* 23, 102–105.
- Chen, B., Xiao, X., Li, X., Pan, L., Doughty, R., Ma, J., Dong, J., Qin, Y., Zhao, B., Wu, Z., Sun, R., Lan, G., Xie, G., Clinton, N., Giri, C., 2017. A mangrove forest map of China in 2015: analysis of time series landsat 7/8 and sentinel-1a imagery in google earth engine cloud computing platform. *ISPRS J. Photogramm. Remote Sens.* 131, 104–120.
- Cortina, J., Maestre, F.T., Vallejo, R., Baeza, M.J., Valdecantos, A., Pérez-Devesa, M., 2006. Ecosystem structure, function, and restoration success: Are they related? *J. Nat. Conserv.* 14 (3-4), 152–160.
- Dai, Z., Mei, X., Darby, S.E., Lou, Y., Li, W., 2018. Fluvial sediment transfer in the Changjiang (Yangtze) river-estuary depositional system. *J. Hydrol.* 566, 719–734.
- Deng, Y., Jiang, W., Tang, Z., Lin, Z., Wu, Z., 2019. Long-Term Changes of Surface Water Bodies in the Yangtze River Basin: Based on the Google Earth Engine Cloud Platform. *Remote Sensing* 11 (19), 2213.
- ESRI 2011. ArcGIS Desktop: Release 10. Redlands, CA: Environmental Systems Research Institute.
- FAO, 2020. Global Forest Resources Assessment 2020: Main report. Rome.
- Fricke, A.T., Nittrouer, C.A., Ogston, A.S., Vo-Luong, H.P., 2017. Asymmetric progradation of a coastal mangrove forest controlled by combined fluvial and marine influence, Cù Lao Dung, Vietnam. *Continental Shelf Res.* 147, 78–90.
- Furukawa, K., Wolanski, E., 1996. Sedimentation in mangrove forests. *Mangroves Salt Marshes* 1 (1), 3–10.
- Gandhi, S., Jones, T., 2019. Identifying mangrove deforestation hotspots in South Asia, southeast Asia and Asia-pacific. *Remote Sensing* 11 (6), 728. <https://doi.org/10.3390/rs11060728>.
- Gao, J., Dai, Z., Mei, X., Ge, Z., Wei, W., Xie, H., Li, S., 2015. Interference of natural and anthropogenic forcings on variations in continental freshwater discharge from the Red River (Vietnam) to sea. *Quat. Int.* 380-381, 133–142.
- Gao, B.-C., 1996. NDWI—A normalized difference water index for remote sensing of vegetation liquid water from space. *Remote Sens. Environ.* 58 (3), 257–266.
- Gedan, K.B., Kirwan, M.L., Wolanski, E., Barbier, E.B., Silliman, B.R., 2011. The present and future role of coastal wetland vegetation in protecting shorelines: answering recent challenges to the paradigm. *Clim. Change* 106 (1), 7–29.
- Giri, C., 2016. Observation and Monitoring of Mangrove Forests Using Remote Sensing: Opportunities and Challenges. *Remote Sensing* 8 (9), 783. <https://doi.org/10.3390/rs8090783>.
- Giri, C., Long, J., Abbas, S., Murali, R.M., Qamer, F.M., Pengra, B., Thau, D., 2015. Distribution and dynamics of mangrove forests of South Asia. *J. Environ. Manage.* 148 (Jan.15), 101–111.
- Giri, C., Ochieng, E., Tieszen, L.L., Zhu, Z., Singh, A., Loveland, T., Masek, J., Duke, N., 2010. Status and distribution of mangrove forests of the world using earth observation satellite data. *Glob. Ecol. Biogeogr.* 20 (1), 154–159.
- Hamilton, S., 2013. Assessing the role of commercial aquaculture in displacing mangrove forest. *Bull. Marine Sci.* 89(2), 585–601(17).
- Hoff, R. Z., Hensel, P., Proffitt, E. C., Delgado, P., Mearns, A.J., 2010. Oil Spills in Mangroves: Planning and Response Considerations.

- Hu, Z., Van Belzen, J., Daphne, V.D.W., Balke, T., Wang, Z.B., Stive, M., Bouma, T.J., 2015. Windows of opportunity for salt marsh vegetation establishment on bare tidal flats: the importance of temporal and spatial variability in hydrodynamic forcing. *J. Geophys. Res. Biogeosci.* 120 (7), 1450–1469.
- Hu, Z., Zhou, J., Wang, C., Wang, H., He, Z., Peng, Y., Zheng, P., Cozzoli, F., Bouma, T.J., 2020. A novel instrument for bed dynamics observation supports machine learning applications in mangrove biogeomorphic processes. *Water Resour. Res.* 56 (7) <https://doi.org/10.1029/2020WR027257>.
- Huang, Z., Zhang, C., Shen, Y., Jiang, S., 2021. Analysis of the climatic characteristics of wind and wave in Weizhou Island sea area. *Marine Forecasts* 38 (2), 62–68.
- Huete, A., Didan, K., Miura, T., Rodriguez, E.P., Gao, X., Ferreira, L.G., 2002. Overview of the radiometric and biophysical performance of the modis vegetation indices. *Remote Sens. Environ.* 83 (1–2), 195–213.
- Jia, M., Wang, Z., Zhang, Y., Ren, C., Song, K., 2015. Landsat-based estimation of mangrove forest loss and restoration in Guangxi Province, China, influenced by human and natural factors. *IEEE J. Sel. Top. Appl. Earth Obs. Remote Sens.* 8 (1), 311–323.
- Jiang, L.M., Chen, B., Qiu, S.F., 2008. The relationship of silt transportation and ocean dynamic condition in Delta of Lianzhou Bay. *J. Guangxi Acad. Sci.* 24 (1), 1–3.
- Kirui, K.B., Kairo, J.G., Bosire, J., Viergever, K.M., Rudra, S., Huxham, M., Briers, R.A., 2014. Mapping of mangrove forest land cover change along the Kenya coastline using Landsat imagery. *Ocean Coastal Manag.* 83, 19–24.
- Kirwan, M.L., Megonigal, J.P., 2013. Tidal wetland stability in the face of human impacts and sea-level rise. *Nature* 504 (7478), 53–60.
- Krauss, K.W., McKee, K.L., Lovelock, C.E., Cahoon, D.R., Saintilan, N., Reef, R., Chen, L., 2014. How mangrove forests adjust to rising sea level. *New Phytol.* 202 (1), 19–34.
- Kuenzer, C., Bluemel, A., Gebhardt, S., Quoc, T.V., Dech, S., 2011. Remote sensing of mangrove ecosystems: a review. *Remote Sensing* 3 (5), 878–928.
- Lee, S.Y., Hamilton, S., Barbier, E.B., Primavera, J., Lewis, R.R., 2019. Better restoration policies are needed to conserve mangrove ecosystems. *Nature Ecol. Evol.* 3 (6), 870–872.
- Lewis, R.R., 2005. Ecological engineering for successful management and restoration of mangrove forests. *Ecol. Eng.* 24 (4), 403–418.
- Lewis, R.R., Brown, B., 2014. Ecological Mangrove Rehabilitation: A Field Manual for Practitioners. Mangrove Action Project – Indonesia, Blue Forests. Canadian International Development Agency and Oxfam, p83.
- Lewis, R.R., Brown, B.M., Flynn, L.L., 2019. Methods and criteria for successful mangrove forest rehabilitation, in: Elsevier (Ed.). *Coastal Wetlands*, pp. 863–887.
- Li, S.H., Xia, H.Y., Chen, M.J., 2001. Study on hydrology and hydrodynamic environment of Guangxi offshore. *Ocean Press* 9–10 pp.
- Li, S.S., Dai, Z.J., Mei, X.F., Huang, H., Wei, W., Gao, J.J., 2017. Dramatic variations in water discharge and sediment load from Nanliu River (China) to the Beibu Gulf during 1960s–2013. *Quaternary International* 440(A): 12–23.
- Long, C.Q., Dai, Z.J., Zhou, X.Y., Mei, X.F., Van, C.M., 2021. Mapping mangrove forests in the Red River Delta, Vietnam. *Forest Ecology and Management* 483.
- Long, J., Napton, D., Giri, C., Graesser, J., 2014. A mapping and monitoring assessment of the Philippines' mangrove forests from 1990 to 2010. *J. Coastal Res.* 294, 260–271.
- Lovelock, C.E., Feller, I.C., Reef, R., Hickey, S., Ball, M.C., 2017. Mangrove dieback during fluctuating sea levels. *Sci. Rep.* 7 (1), 1680.
- Lovelock, C.E., Cahoon, D.R., Friess, D.A., Guntenspergen, G.R., Krauss, K.W., Reef, R., Rogers, K., Saunders, M.L., Sidik, F., Swales, A., Saintilan, N., Thuyen, L.X., Triet, T., 2015. The vulnerability of Indo-Pacific mangrove forests to sea-level rise. *Nature* 526 (7574), 559–563.
- Lovelock, C.E., Reef, R., Masqué, P., 2021. Vulnerability of an arid zone coastal wetland landscape to sea level rise and intense storms. *Limnol. Oceanogr.* 1–14.
- Luo, Z.R., Ying, Z.F., Yang, G.R., Wang, H.S., Luo, X.L., Tian, X.P., 1992. The harbours in South China. Sun Yat-sen University Pre, p. 193 pp.
- Mbense, S., Rajkaran, A., Bolosha, U., Adams, J., 2016. Rapid colonization of degraded mangrove habitat by succulent salt marsh. *South Afr. J. Bot.* 107, 129–136.
- McIvor, A.L., Spencer, Moller, Spalding, 2013. The response of mangrove soil surface elevation to sea level rise. *Nature Conservancy and Wetlands International*.
- McKee, K.L., Cahoon, D., Feller, I.C., 2007. Caribbean mangroves adjust to rising sea level through biotic controls on change in soil elevation. *Glob. Ecol. Biogeogr.* 16 (5), 545–556.
- Milliman, J. D. and Farnsworth, K. L., 2011. River Discharge to the Coastal Ocean – A Global Synthesis.
- Morris, J.T., Sundareshwar, P.V., Nietch, C.T., Cahoon, B.K.R., 2002. Responses of coastal wetlands to rising sea level. *Ecology*, 83(10), 2869–2877.
- Murray, B.C., 2012. Economics: Mangroves' hidden value. *Nat. Clim. Change* 2 (11), 773–774.
- Nicholls, R.J., Cazenave, R., 2010. Sea-level rise and its impact on coastal zones. *Science* 328 (5985), 1517–1520.
- Rajkaran, A., Adams, J., 2012. The effects of environmental variables on mortality and growth of mangroves at Mngazana Estuary, Eastern Cape, South Africa. *Wetl. Ecol. Manag.* 20 (4), 297–312.
- Raw, J.L., Godbold, J.A., Niekerk, L.V., Adams, J.B., 2019. Drivers of mangrove distribution at a high-energy, wave-dominated, southern range limit. *Estuarine Coastal and Shelf Science* 226, 106296.1–106296.8.
- Richards, D.R., Friess, D.A., 2015. Rates and drivers of mangrove deforestation in Southeast Asia, 2000–2012. *PNAS* 113 (2), 344–349.
- Rouse, J.W., Haas, R.H., Scheel, J.A., and Deering, D.W., 1974. Monitoring Vegetation Systems in the Great Plains with ERTS. *Proceedings, 3rd Earth Resource Technology Satellite (ERTS) Symposium* 1, 48–62.
- Sánchez-Núñez, D.A., Bernal, G., Pineda, J., 2019. The relative role of mangroves on wave erosion mitigation and sediment properties. *Estuaries Coasts* 42 (8), 2124–2138.
- Scott, L.M., Janikas, M.V., 2010. In: *Handbook of Applied Spatial Analysis*. Springer Berlin Heidelberg, Berlin, Heidelberg, pp. 27–41. https://doi.org/10.1007/978-3-642-03647-7_2.
- Song, D.H., Bao, X.W., Zhang, S.F., Zhang, C.H., 2012. Three-dimensional numerical simulation of tides and tidal currents in the Lianzhou Bay and adjacent areas. *Marine Sci. Bull.* 15, 1–15.
- Swales, A., Bentley, S.J., 2008. Recent tidal-flat evolution and mangrove-habitat expansion: application of radioisotope dating to environmental reconstruction. *Sediment dynamics in changing environments: International Association of Hydrological Sciences Publication* 325, 76–84.
- Swales, A., Reeve, G., Cahoon, D.R., Lovelock, C.E., 2019. Landscape evolution of a fluvial sediment-rich *Avicennia marina* mangrove forest: insights from seasonal and inter-annual surface-elevation dynamics. *Ecosystems* 22, 1232–1255.
- Syvitski, J.P.M., Kettner, A.J., Overeem, I., Hutton, E.W.H., Hannon, M.T., Brakenridge, G.R., Giosan, L., 2009. Sinking deltas due to human activities. *Nature Geoscience* 2 (10), 681–686.
- Tang, R., Dai, Z., Zhou, X., Li, S., 2021. Tropical cyclone-induced water and suspended sediment discharge delivered by mountainous rivers into the Beibu Gulf South China. *Geomorphol.* 389, 107844. <https://doi.org/10.1016/j.geomorph.2021.107844>.
- Thomas, N., Bunting, P., Lucas, R., Hardy, A., Rosenqvist, A., Fatoyinbo, T., 2018. Mapping mangrove extent and change: a globally applicable approach. *Remote Sens.* 10 (9), 1466.
- Van Santen, P., Augustinus, P.G.E.F., Janssen-Stelder, B.M., Quartel, S., Tri, N.H., 2007. Sedimentation in an estuarinemangrove system. *J. Asian Earth Sci.* 29 (4), 566–575.
- Wang, R.M., Dai, Z.J., Huang, H., Long, C.Q., Liang, X.X., Li, S.S., 2021. Research on biogeomorphic processes of *Aegiceras corniculatum* in the Nanliu River Estuary. *Haiyang Xuebao* 43 (10), 1–13.
- Wang, X., Xiao, X., Zou, Z., Hou, L., Qin, Y., Dong, J., Doughty, R.B., Chen, B., Zhang, X., Chen, Y., Ma, J., Zhao, B., Li, B., 2020. Mapping coastal wetlands of China using time series landsat images in 2018 and google earth engine. *ISPRS J. Photogramm. Remote Sens.* 163, 312–326.
- Webb, E.L., Friess, D.A., Krauss, K.W., Cahoon, D.R., Guntenspergen, G.R., Phelps, J., 2013. A global standard for monitoring coastal wetland vulnerability to accelerated sea-level rise. *Nat. Clim. Change* 3, 458–465.
- Wolanski, E., Williams, D., Hanert, E., 2006. The sediment trapping efficiency of the macro-tidal Daly Estuary, tropical Australia. *Estuar. Coast. Shelf Sci.* 69 (1–2), 291–298.
- Woodroffe, C.D., 1995. Response of tide-dominated mangrove shorelines in northern Australia to anticipated sea-level rise. *Earth Surface Processes and Landforms*, 20(1), 65–85.
- Woodroffe, C.D., Rogers, K., McKee, K.L., Lovelock, C.E., Mendelsohn, I.A., Saintilan, N., 2016. Mangrove sedimentation and response to relative sea-level rise. *Ann. Rev. Marine Sci.* 8 (1), 243–266.
- Worthington, T.A., Ermgassen, P., Friess, D.A., Krauss, K.W., Lovelock, C.E., Thorley, J., Tingey, J., Woodroffe, C.D., Bunting, P., Cormier, N., Lagomasino, D., Lucas, R., Murray, N., Sutherland, W.J., Spalding, M., 2020. A global biophysical typology of mangroves and its relevance for ecosystem structure and deforestation. *Sci. Rep.* 10 (1), 14652.
- Xiong, Y., Jiang, Z., Xin, K., Liao, B., Chen, Y., Li, M., Guo, H., Xu, Y., Zhai, X., Zhang, C., 2021. Factors influencing mangrove forest recruitment in rehabilitated aquaculture ponds. *Ecol. Eng.* 168, 106272. <https://doi.org/10.1016/j.ecoleng.2021.106272>.
- Yang, G.R., Li, C.C., Luo, Z.R., Ying, Z.F., 1995. Research on coastal dynamic geomorphology and its application in port construction of South China. Sun Yat-sen University Pre 41 pp.
- Zhao, Y., Xie, Q., Lu, Y., Hu, B., 2017. Hydrologic evaluation of TRMM multisatellite precipitation analysis for Nanliu River Basin in humid Southwestern China. *Sci. Rep.* 7 (1), 2470.